The boron-oxygen (B_iO_i) defect complex induced by irradiation with 23 GeV protons in p-type epitaxial silicon diodes

C. Liao, E. Fretwurst, E. Garutti, J. Schwandt, M. Moll, A. Himmerlich, Y. Gurimskaya, I. Pintilie, A. Nitescu Z. Li, L. Makarenko

***Abstract*—In this work the Thermally Stimulated Current (TSC) technique has been used to investigate the properties of the radiation induced B_iO_i (interstitial Boron - B_i, interstitial Oxygen - O_i) defect complex by 23 GeV (E_{kin}) protons, including activation energy, defect concentration as well as the annealing behavior. At first isothermal annealing (at 80 ^{o}C for 0 to 180 minutes) followed by isochronal annealing (for 15 minutes between 100 ^{o}C and 190 ^{o}C in steps of 10 ^{o}C) studies had been performed in order to get information about the thermal stability of the B_iO_i defect in 50 Ωcm material after irradiation with 23 GeV protons to a fluence of 6.91×10^{13} p/cm^2. The results are presented and discussed. Furthermore, the extracted data from TSC measurements are compared with the macroscopic properties derived from current-voltage (I-V) and capacitance-voltage (C-V) characteristics. In addition, the introduction rate of B_iO_i as function of the initial doping concentration was determined by exposing diodes with different resistivities (10 Ωcm, 50 Ωcm, 250 Ωcm, and 2 kΩcm) to 23 GeV protons. These results are compared with data from TSC and DLTS measurements achieved by the team of the CERN-RD50 "Acceptor removal project".**

***Index Terms*—B_iO_i defect, proton irradiation, introduction rate, TSC technique, annealing.**

I. Introduction

In the frame of the CERN-RD50 collaboration new types of silicon sensors for the High Luminosity Large Hadron Collider (HL-LHC) experiments are under development and detailed investigation in order to cope with the extraordinary high particle rate – up to 200 pile up events per bunch crossing – and the related large radiation damage effects in the sensors. The new types of sensors which are recently developed are so called Low Gain Avalanche Detectors (LGADs) for high precision timing and position resolution [1], [2] and High Voltage CMOS devices (HV CMOS) for the inner tracking detectors [3] – [8]. Both types of these sensors as well as the new pixel and strip devices will be manufactured on boron doped (p-type) silicon. The degradation of the performance of these sensors due to the expected high radiation field, and a search for a possible improvement of their radiation tolerance by defect engineering is of high relevance. For example the exposure of LGADs to radiation leads to a reduction of the gain with increasing particle fluence [1], [2], [9]. This degradation is caused by a deactivation of the boron in the highly doped p-type layer ($\approx 1 \times 10^{16}$ cm^{-3}), the gain layer, which leads to a reduction of the space charge and consequently a lowering of the electric field followed by a decrease of charge multiplication in this layer. In general the deactivation of the boron dopant is called acceptor removal.

The reason for the deactivation of the boron acceptor by radiation is the generation of defect complexes that contain boron which are either not electrically active or exhibit deep energy levels in the band gap and, therefore, cannot act as shallow dopants. These defect complexes can be detected by spectroscopic methods like Thermally Stimulated Current (TSC) and Deep Level Transient Spectroscopy (DLTS).

In this paper we will report at first in section II on the experimental details about the used p-type epitaxial diodes of different resistivities, the irradiation with 23 GeV protons and the methods for the investigation of the macroscopic and microscopic properties of the devices. In section III the results of the current-voltage and capacitance-voltage measurements are presented. The microscopic measurements using the Thermally Stimulated Current (TSC) technique with the focus on the Boron-Oxygen (B_iO_i) defect complex, its correlation with the radiation induced change of the effective space charge density and annealing behavior are described and discussed in section IV, including finally the generation rates as function of the initial boron content in the devices will be given.

II. Experimental details

A set of 50 µm thick p-type epitaxial layers with different resistivity between 10 Ωcm and 2000 Ωcm (see TABLE I) were grown on highly boron-doped Cz substrates ($\rho \approx 0.003$ Ωcm) by ITME [10] and pad-sensors with a sensitive area of 2.632×2.632 mm^2 have been processed by CiS [11]. The pad is surrounded by a current collection ring and several guard rings. For a possible light injection also into the rear side of the diode a 3×3 mm^2 cavity was etched into the Cz substrate down to the EPI layer and a circular opening was processed with a diameter of 1.2 mm in the metallization.

C. Liao, E. Fretwurs, E. Garutti and J. Schwandt are with the Institute for Experimental Physics, University of Hamburg, Luruper Chaussee 149, 22761 Hamburg, Germany e-mail: (chuan.liao@desy.de), (eckhart.fretwurst@desy.de), (erika.garutti@physik.uni-hamburg.de), (joern.schwandt@desy.de).

A. Himmerlich, Y. Gurimskaya, and M. Moll are with CERN. e-mail: (anja.himmerlich@cern.ch), (yana.gurimskaya@cern.ch), (Michael.Moll@cern.ch).

L. Makarenko is with Belarussian State University. e-mail: (makarenko@bsu.by).

I. Pintilie and A Nitescu are with National Institute of Materials Physics, Atomistilor 405A, Magurele 077125, Romania. e-mail: (ioana@infim.ro).

Z. Li is with college of physics and optoelectronic engineering, Ludong University, Yantai, 264025, China and school of optoelectronic engineering, Zaozhuang university 277160, China email: (3636@ldu.edu.cn).

The irradiation with 23 GeV protons was performed at the CERN-PS IRRAD facility and the achieved 1 MeV neutron equivalent fluence values Φ_{eq} are included in TABLE I.

The macroscopic device performance of the investigated diodes was measured by means of current-voltage (I-V) and capacitance-voltage (C-V) characteristics. The radiation induced changes in the effective doping concentration (N_{eff}) and the full depletion voltage V_{fd} were determined from C-V measurements using different frequencies (230 Hz, 445 Hz, 1 kHz and 10 kHz) and guard ring grounded.

For the characterization of the radiation induced electrically active defects the Thermally Stimulated Current (TSC) method was used [12] – [16]. The TSC experimental procedure consists of cooling down (0 V) the sample to low temperatures (typically 10 K) where filling of the defects is performed by forward biasing of the diode. A TSC spectrum is then recorded by measuring the diode current during heating up the device with a constant rate of 0.183 K/s under reverse bias applied to the diode [15]. The guard ring was always grounded and the time step for the read-out of the current and temperature was set by the software to 1 s. Isothermal annealing experiments were performed at a temperature of 80 °C for all irradiated diodes and the macroscopic as well as the microscopic properties evaluated. For one 50 Ωcm diode isochronal annealing in the temperature range from 100 °C to 190 °C in steps of 10 °C for 15 min at each step was studied in order to get information on the thermal stability of the specific B_iO_i defect which is responsible for the acceptor removal effect in this material.

III. I-V, C-V MEASUREMENT

In this section the properties and parameter of the measured I-V and C-V characteristics of the irradiated sensors are presented and discussed.

As an example in Fig. 1a I-V curves of the diode 06-71 (50 Ωcm material) for different annealing steps are shown. The measurement temperature was always 20 °C and the guard ring connected to ground. After full depletion the current is still increasing which might be due to the high electric field at the n^+ - p junction which is in order of 10^5 V/cm for a bias voltage of 300 V leading to a possible trap assisted tunneling effect [17]. But a contribution of surface current from interface traps of the oxide layer surrounding the pad cannot be excluded [18]. The full depletion voltage V_{fd} for the annealing steps between 0 min and 180 min at 80 ^{o}C are indicated as red stars in Fig. 1a. The values increase from (168 ± 1) V to (188 ± 1) V for 0 min and 8 min and decrease slightly for large annealing times to value of (179 ± 1) V at 80 ^{o}C. For the annealing steps between as irradiated and 180 min at 80 ^{o}C a strong decrease of the current is measured, which is a well-known observation for hadron irradiated silicon sensors and mainly due to the annealing property of the radiation induced three-vacancy (V_3) defect [19]. A characteristic parameter for the radiation induced generation current ΔI is the so-called current related damage parameter α defined by:

$$\alpha(T_{ann}, t_{ann}) = \frac{\Delta I}{Vol \times \Phi_{eq}} \quad (1)$$

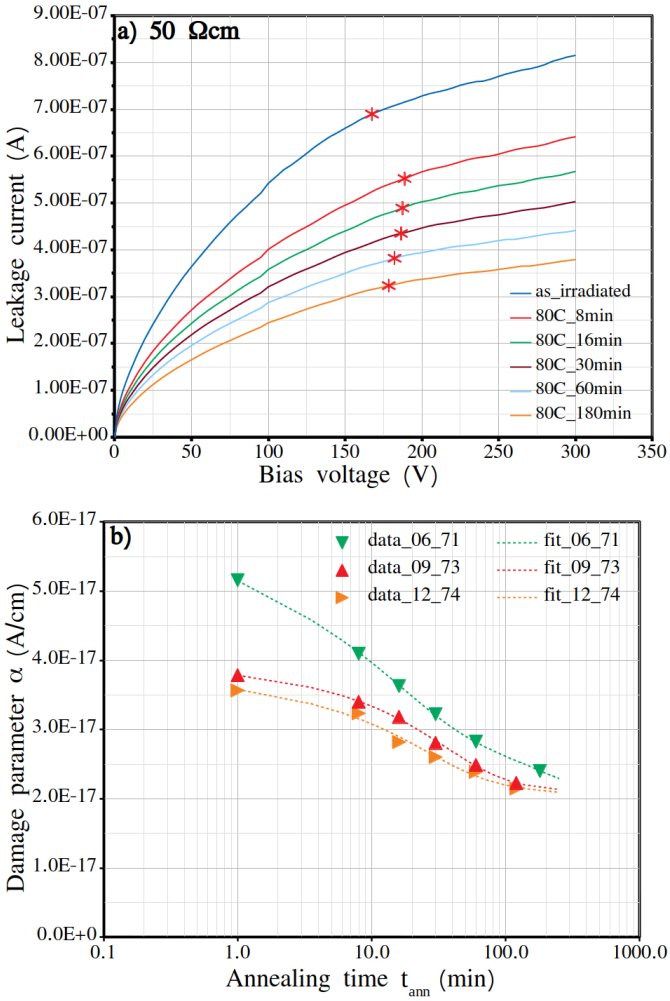

Figure 1: (a) Current-voltage characteristics of 50 Ωcm diode (06-71) for different annealing steps at 80 ^{o}C up to 180 min are plotted. The red asterisks in the I-V curves indicate the full depletion voltages at which the current related damage parameter α are determined. Measurement parameter: Φ_{eq} = 4.28×10^{13} cm^{-2}, measurement temperature: 20^{o}C, humidity $\leq$ 10%. (b) Current related damage parameter $\alpha(T_{ann}, t_{ann})$ versus annealing time t_{ann} at 80 ^{o}C for 3 diodes with different initial resistivity (06-71 - 50 Ωcm, 09-73 - 250 Ωcm, 12-74 - 2 kΩcm). The dashed lines are fits to the data according to eq.(2)

where Vol is the depleted volume of the device, Φ_{eq} the 1 MeV neutron equivalent fluence, T_{ann} the annealing temperature and t_{ann} the annealing time. A parameterization of the time dependence is given by [15]:

$$\alpha(t_{ann}) = \alpha_I \exp\left(-\frac{t_{ann}}{\tau_I}\right) + \alpha_0 - \beta \ln\left(\frac{t_{ann}}{t_0}\right) \quad (2)$$

with amplitude α_I and the time constant τ_I of the short term component, the constant term α_0, the parameter β of the logarithmic term with t_0 = 1 min. The dependence of the parameter on the annealing temperature can be found in [15]. Fig. 1b shows the α values extracted from the I-V curves (at $V \approx V_{fd}$) as function of annealing time and the corresponding

TABLE I

Device information ($N_{eff,0}$ from spreading resistivity measurement performed by ITME)

Label	Diode 01-73	Diode 06-71	Diode 09-73	Diode 12-74
Nominal resistivity ρ (Ωcm)	10	50	250	2000
Initial doping $N_{eff,0}$ (cm^{-3})	1.37×10^{15}	1.97×10^{14}	4.53×10^{13}	6.24×10^{12}
Radiation fluence Φ_{eq} (cm^{-2})	4.28×10^{13}			
Area A (cm^2)	0.06927			
Geometric thickness D (μm)	50			

fits according to eq.(2). The parameters of the fitted curves are presented in TABLE II. The estimated errors of the parameters in eq.(2) are caused by systematic uncertenties in the voltage at which the current data were taken due to the large increase of the I-V curves near and above the full depletion voltage.

The other macroscopic property which is affected by radiation is the effective space charge density N_{eff} or full depletion voltage V_{fd} of the device. Both quantities have been extracted from C-V characteristics measured at frequency of 10 kHz, an AC signal amplitude of 0.5 V and in parallel mode operation of the LCR-meter. For the evaluation of the full depletion voltage V_{fd} it is a common procedure to perform linear fits to the rising part of the $1/C^{-2}$ - V curve in a proper voltage range and the saturation part above full depletion (see Fig. 2a). The voltage of the crossing point is then taken as V_{fd}. But such procedure is only valid if N_{eff} is constant throughout the entire sensor volume and the concentration of free charge carriers is large compared to the concentration of traps in the bulk. The $1/C^{-2}$ - V curves measured for the 50 Ωcm diode after different annealing steps is demonstrated in Fig. 2a. The effective space charge concentration N_{eff} can then be calculated in two ways:

$$N_{eff} = \frac{2\varepsilon_0\varepsilon_r V_{fd}}{q_0 d^2} \quad (3)$$

$$N_{eff}(V) = \frac{2}{\varepsilon_0\varepsilon_r A^2 q_0 \frac{d(1/C^2)}{dV}} \quad (4)$$

where ε_0 is the permittivity of vacuum, ε_r the relative permittivity of silicon (11.9), q_0 the elementary charge, A the active pad area and d the depleted depth for full depletion, which is derived from:

$$w(V) = \frac{\varepsilon_0\varepsilon_r A}{C(V)}, \quad V < V_{fd} \quad (5)$$

Where for $V = V_{fd}$ the depletion depth is given by $w(V_{fd}) = d$ and the capacitance $C_{fd} = \varepsilon_0\varepsilon_r A/d$. The full depletion voltages extracted from $1/C^{-2}$ - V curves for the high resistivity diode (2 kΩcm, 12-74) are very small in the range from about 4 V to 5 V for the annealing steps between 0 min to 120 min and for the 250 Ωcm diode (09-73) V_{fd} varies between 15 V to 20 V.

For C-V measurements the guard ring was grounded and the measurements were performed at 20 °C.

According to eq.(4) and eq.(5), the doping profiles are calculated for diodes with different resistivities (10 Ωcm, 50 Ωcm, 250 Ωcm and 2 kΩcm) and annealing time of 30 min at 80 ^{o}C, as shown in Fig. 2b. In this figure the range of the depletion depth (2 μm to 10 μm for 10 Ωcm and 10 μm to 35 μm for the other diodes) for evaluating the mean values of N_{eff} is also indicated. Finally, the extracted values N_{eff} as function of annealing time for most devices are plotted in Fig. 3. Both equations (3) and (4) are approximately valid for non-irradiated diodes under the assumption of an abrupt n^+ - p junction and a homogeneously distributed space charge density. But it has to mentioned that there are several shortcomings for irradiated devices. For example in radiation damaged diodes the effective space charge might be non-homogeneous leading to complex electric field distributions, the influence of strong changes in free charge carrier concentrations on the evaluation of the depletion depth [20] or frequency dependence of C-V measurements for highly irradiated sensors especially observed in high resistivity material [21]. While for the irradiated diodes (Φ_{eq} = 4.28×10^{13} cm^{-2}) with a resistivity of 10 Ωcm and 50 Ωcm a frequency dependence in C-V measurements is not observed in the higher resistivity material (250 Ωcm and 2 kΩcm) a frequency dependence is seen. Considering these effects the differences in the evaluated N_{eff} values for the 50 Ωcm diode by using eq.(3) and eq.(4) are estimated to below 3 % for the different annealing steps. Using only eq.(4) the deviations are below 1 % if the voltage ranges are chosen properly (10 V to 100 V for 50 Ωcm, 4 V to 10 V for 250 Ωcm and about 1 V to 3 V for 2 kΩcm depending on the annealing step). Much larger differences in N_{eff} up to 17 % are found for the 2 kΩcm material taking the data measured at frequencies of 230 Hz and 10 kHz and using eq.(3). On the other hand the evaluation according to eq.(4) results for both frequencies much smaller differences in the order of 3 %.

As can be seen in Fig. 3, the changes of N_{eff} versus annealing time at 80 °C are quite small. Only for the high resistivity diode (2 kΩcm) an increase of N_{eff} is observed. These results can be explained by the thermal stability of the radiation induced boron related defect B_iO_i and are discussed in the next section.

IV. TSC MEASUREMENTS FOR B_iO_i DEFECT

The Thermally Stimulated Current (TSC) technique has been used to investigate the properties of the radiation induced B_iO_i defect complex by 23 GeV protons, including activation energy, defect concentration as well as the annealing behavior.

As an example Fig. 4a shows TSC spectra of the irradiated diodes with different resistivities (10 Ωcm, 50 Ωcm, 250 Ωcm, 2 kΩcm). The spectrum of the 10 Ωcm diode was recorded at 100 V and normalized to the fully depleted depth by a factor d/w(V). All other spectra were taken at voltages above fully depletion (see caption Fig. 4a). Fig. 4b shows TSC spectra of the irradiated diode 06-71 (initial resistivity of 50 Ωcm, see TABLE I) for different applied bias voltages in the range between 100 V and 300 V during heating up. The observed

TABLE II

Current related damage parameter

Label	Diode 06-71	Diode 09-73	Diode 12-74	Reference [15]
Nominal resistivity	50 Ωcm	250 Ωcm	2 kΩcm	100 Ωcm - 7 kΩcm
α_I (1×10^{-17} A/cm)	1.00 ± 0.1	1.29 ± 0.1	1.00 ± 0.1	1.13
τ_I (min)	17.22 ± 2	35.11 ± 3	26.17 ± 2	9
α_0 (1×10^{-17} A/cm)	4.21 ± 0.2	2.53 ± 0.2	2.62 ± 0.2	4.23
β (1×10^{-18} A/cm)	3.47 ± 0.3	0.71 ± 0.02	0.95 ± 0.1	2.83

dominant peaks in the temperature range of 90 K to 100 K and their shifts to lower temperature with increasing bias voltage are attributed to the B_iO_i defect. Such assignment was presented by different authors who investigated radiation induced defects in boron doped material [22]- [24]. The main arguments are that the introduction of this defect depends on the boron, carbon and oxygen content in the material, that the defect kinetics rate depends on the ratio of the oxygen concentration to the boron concentration ([22], [24]). Also theoretical calculations are in accordance with these properties [23]. This voltage dependence of the shift of the peak maximum is a typical property of so-called coulombic centers which are governed by the Poole-Frenkel effect [25] – [27] that means an electrical field dependence of the emission rate or the activation energy of the defect center, respectively. This will be described in more detail in the next paragraph. Another observation is the increasing peak amplitude of the B_iO_i complex with bias which is due to firstly an increase of the depletion depth before fully depletion and thereafter for higher voltages an extension of the depleted region into the p^+ backside of the highly doped substrate.

A. Some theoretical background of TSC

The general formalism of the TSC technique is in detail described in the literature [12] – [16]. The general formula for a single electron trap existing in N_t concentration in a full depleted diode is given by:

$$I^e_{TSC}(T) = \frac{1}{2} \cdot q_0 \cdot A \cdot d \cdot e_n(T) \cdot n_t(T_0) \cdot f\,(T) \quad (6)$$

$$e_n = \sigma_n \cdot v_{th,n} \cdot N_C \cdot \exp\left(-\frac{E_a}{k_B T}\right) \quad (7)$$

$$e_p = \sigma_p \cdot v_{th,p} \cdot N_V \cdot \exp\left(-\frac{E_a}{k_B T}\right) \quad (8)$$

$$f(T) = \exp\left(-\frac{1}{\beta}\int_{T_0}^{T} (e_n(T') + e_p(T'))\, dT'\right) \quad (9)$$

where q_0 is the elementary charge, T the temperature, A the active area, d the fully depleted depth, e_n and e_p are the emission rate for electrons and holes. N_C and N_V are the density of states in the conduction band and valence band, respectively and are taken from [28]. The activation energy for electrons is $E_a = E_C$ - E_t and for holes $E_a = E_t$ - E_V, where E_t is energy level of the electrons or holes trap and $E_{C,V}$ the conduction and valence band edge, respectively. $\sigma_{n,p}$ are capture cross section for electrons and holes, $v_{th,n,p}$ are the thermal velocities for electrons and holes taken from [28]. k_B is the Boltzmann constant, $f(T)$ describes the fraction of defects occupied by electrons at temperature T, β is the heating rate and $n_t(T_0)$ is the density of defects that are filled with electrons at T_0.

In the investigated p-type diodes, the B_iO_i defect on which this study is focusing is detected in a TSC experiment only if electrons can be injected at low temperature. This is done by forward biasing the diodes at 10 K, by injecting both electrons and holes. In the hypothesis that equal amounts of electrons and holes are injected during the forward biasing the density of defects filled with electrons is given by [16]:

$$n_t(T_0) = N_t \frac{c_n}{c_n + c_p} \quad (10)$$

where c_n and c_p are capture coefficients for electrons and holes, respectively ($c_{n,p} = \sigma_{n,p}\ v_{th,n,p}$). N_t is the total defect concentration in the bulk. For the B_iO_i defect the capture cross sections σ_n and σ_p had been measured [22], [29] and values of 1×10^{-14} cm^2 and 1×10^{-20} cm^2 were derived. Therefore σ_p and c_p can be neglected in eq.(8), eq.(9) and eq.(10). Thus, the B_iO_i TSC signal can be approximated by:

$$I^e_{TSC}(T) = \frac{1}{2} \cdot q_0 \cdot A \cdot d \cdot e_n \cdot N_t \cdot f\,(T) \quad (11)$$

$$f(T) = \exp\left(-\frac{1}{\beta}\int_{T_0}^{T} e_n(T')\, dT'\right) \quad (12)$$

For coulombic trap centers like the B_iO_i the emission rate e_n is not anymore a constant quantity with respect to the applied bias voltage but becomes field dependent. The 3D Poole-Frenkel effect in the emission rate e_n is given by [25] – [27]:

$$e^{pf}_n = e_{n0}(T) \cdot \left[\left(\frac{1}{\gamma^2}\right)(e^{\gamma}(\gamma - 1) + 1) + \frac{1}{2}\right] \quad (13)$$

$e_{n,0}(T)$ denotes the field independent emission rate with the so-called zero field activation energy $E_a = E_{a,0}$ and $\gamma = (q_0|\vec{E}|/(\pi\varepsilon_0\varepsilon_r))^{\frac{1}{2}} q_0/(k_B T)$. $|\vec{E}|$ is the electric field in the sensor bulk and is position dependent. In this case the TSC current is given by:

$$I_{TSC} = \frac{1}{2} q_0 A w(V,T) N_t e^{pf}_n \exp\left(-\frac{1}{\beta}\int_{T_0}^{T} e^{pf}_n(T')\, dT'\right) \quad (14)$$

In this equation the position dependent electric field is not taken into account. As a first approximation the average value $\langle|\vec{E}|\rangle = V/w$ is applied.

If the diode is not fully depleted the value d has to be exchanged by the depleted width $w(V,T)$ which depends on the applied bias voltage V and temperature T. The temperature dependence of w is mainly neglected if the concentration of the trap is small compared to the overall space charge concentration in the T range of interest. Another effect influencing

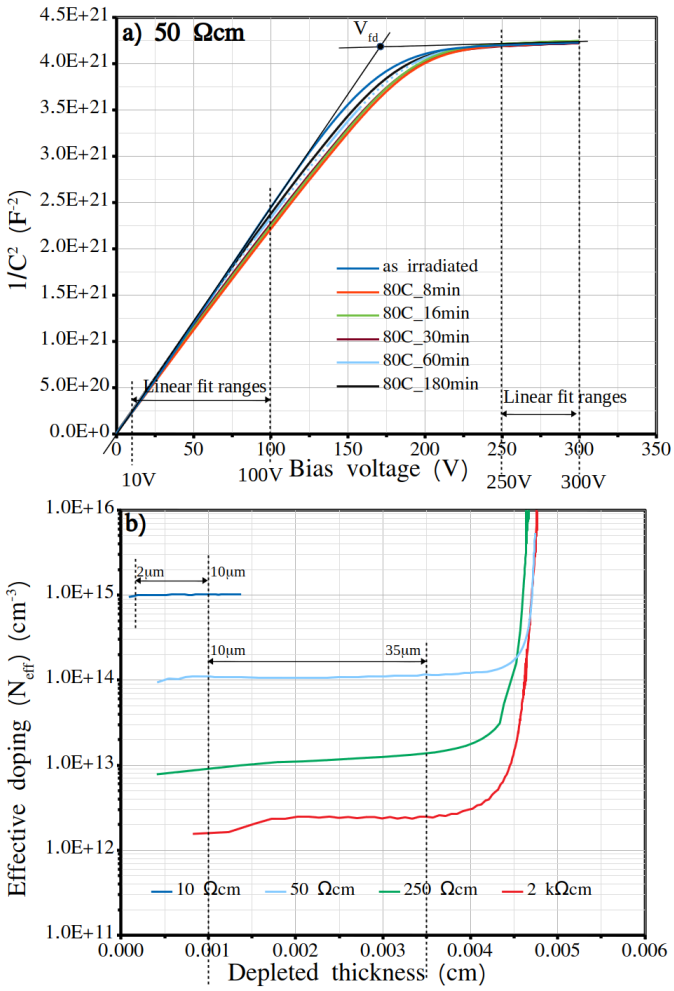

Figure 2: (a) $1/C^{-2}$ - V curves for 50 Ωcm diode (06-71) for all annealing steps at 80 ^{o}C. Measurement parameter: measurement temperature T = 20 ^{o}C, frequency f = 10 kHz, humidity $\leq$ 10%, V_{AC} = 0.5 V. The voltage ranges of the linear fits in the rising and saturation part of the curve for 0 min at 80 ^{o}C are indicated and the crossing point of the straight lines at V_{fd}. (b) Doping profiles of the diodes with different resistivity are shown for an annealing of 30 min at 80 ^{o}C. The profiles were evaluated from C-V measurements by using eq.(4) and eq.(5). The mean values of N_{eff} are derived from the indicated depth ranges and are presented in Fig. 3.

the peak shape is a possible cluster effect [30], [31] which leads to a dependence of the activation energy $E_a(T)$ on the trap occupation $f(T)$. For an attractive Coulomb interaction this results in:

$$E_a(T) = E_{a0} + (1 - f(T))\Delta E_a \quad (15)$$

The value of the energy shift ΔE_a depends on the density of charged traps inside the cluster. However the results of ΔE_a extracted from B_iO_i peak (see TABLE III) indicate that the B_iO_i is a point defect.

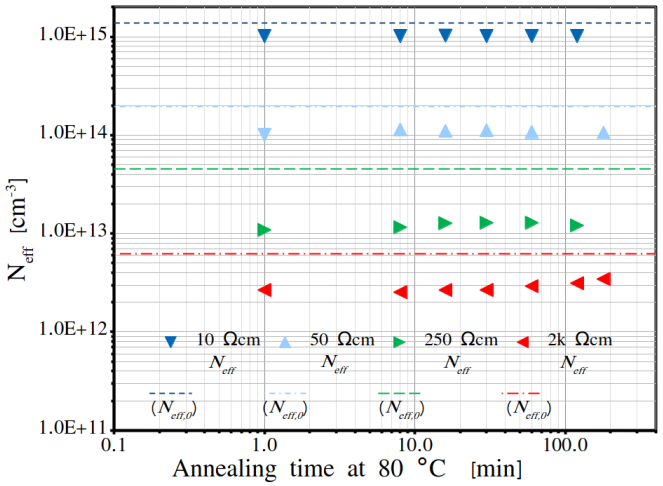

Figure 3: Development of the effective doping concentration N_{eff} with annealing time for 50 µm thick epitaxial diodes of different resistivities (see legend) after irradiation with 23 GeV protons to $\Phi_{eq} = 4.28 \times 10^{13}$ cm^{-2}. The dashed lines indicate the initial doping concentration $N_{eff,0}$ of the different diodes.

B. *Extract parameter for B_iO_i from TSC measurements*

In order to reproduce the TSC peak of the B_iO_i defect in all measured spectra of the irradiated diodes with different resistivities the data were fitted according to eq.(14), taking the cluster effect (eq.(15)) into account. For the fitting procedures the temperature ranges of the B_iO_i TSC peak are chosen to T_{max} - 2 K and T_{max} + 4 K where T_{max} corresponds to the temperature at the maximum value of the TSC peak. There are 3 free parameter - zero field activation energy E_{a0}, cluster related energy shift ΔE_a and the defect concentration N_t - which are extracted from the fits. The capture cross section σ_n = 1×10^{-14} cm^2 [22], [29] was fixed in the fitting routine. The resulting parameters are summarized in TABLE III for three diodes with different resistivities and different annealing steps. It should be mentioned here that the low temperature tail of the B_iO_i peak could not be reproduced by the fitting routine, especially at higher bias voltages (Fig. 4b). Therefore, it was supposed that in this temperature range a further unknown defect might be hidden. In order to clarify this problem TSC studies were performed by changing the filling temperature T_0 in the range 10 K - 70 K. From Fig. 5a it is obvious that indeed a defect (labeled as X-defect) is showing up in that region with increasing peak height for larger T_0. Specific studies on this defect resulted in the fact that it is a hole trap showing a strong Poole-Frenkel effect with a zero field energy level of $E_{a0} = E_t$ - $E_V \approx$ 0.21 eV. Fig. 5b shows the concentration of the B_iO_i and the X-defect as function of T_0. While the B_iO_i concentration exhibits only a small increase with T_0 the change of the X-defect concentration is much stronger. More information about the X-defect can be found in reference [32].

The extracted zero field activation energies E_{a0} as function of the applied bias voltage are presented for the 250 Ωcm and 2 kΩcm diode (09-73, 12-74) in Fig. 6 for the different isothermal annealing steps, respectively. The E_{a0} values presented

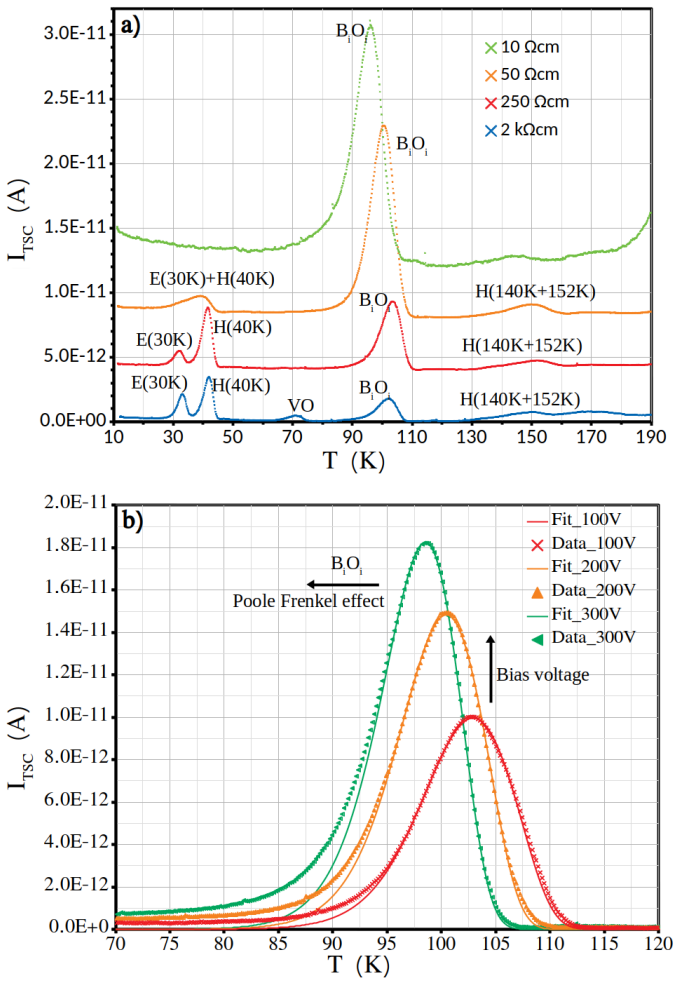

Figure 4: (a) TSC spectra of diodes with different resistivity after 23 GeV proton irradiation to $\Phi_{eq} = 4.3 \times 10^{13}$ cm^{-2} for reverse bias 20 V (2 kΩcm), 40 V (250 Ωcm), 200 V (50 Ωcm) and 100 V (10 Ωcm, spectrum normalized to d/w(100 V)). TSC parameters: T_0 = 10 K, V_{fill} = 5 V, heating rate β = 0.183 K/s. For clarity, the individual curves are shifted vertically by 4 pA. (b) TSC spectra of 50 Ωcm diode (06-71) for different bias voltages (V) during heating up and after annealing for 16 min at 80 ^{o}C. TSC parameters are the same as presented in (a).

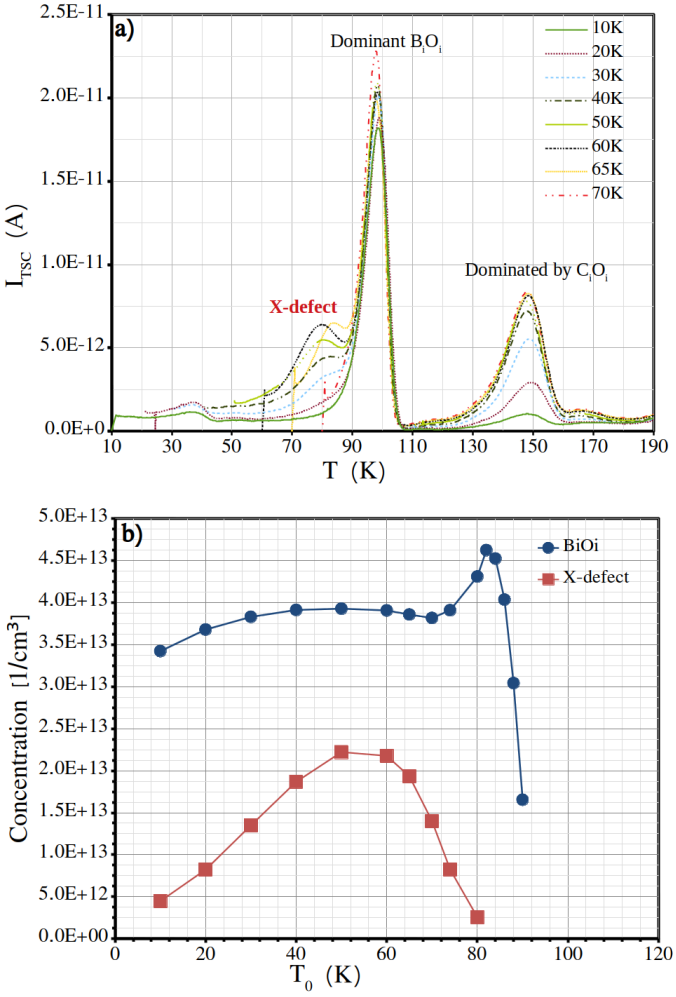

Figure 5: (a) TSC spectra for different T_0 of 50 Ωcm diode after 23 GeV proton irradiation. Annealing step t_{ann} = 30 min, T_{ann} = 80 ^{o}C. Experimental parameter of TSC: V_{fill} = 5 V, V = 250 V. (b) Concentration of B_iO_i and X-defect versus filling temperature T_0 extracted from the TSC spectra shown above.

in TABLE III show a dependence on the material resistivity and annealing step. This might be due to the different applied bias voltages for the different diodes leading to different electric field strength values which are highest in the 50 Ωcm one. Another effect could be caused by the X-defect which contribute partly to the B_iO_i signal, especially for the 50 Ωcm diode. A slight voltage dependence is observed as well as some changes with the annealing time. Further, it should be mentioned that the values given in TABLE III are mean values with respect to all results gained from the analysis of different bias voltages. The errors depend on fitting ranges. Both errors are based on the assumption that the temperature dependent of σ and w can be neglected.

Further, the unexpected increases of the B_iO_i concentration ($[B_iO_i]$) for bias voltages higher than the voltage for full depletion as shown in Fig. 7 for the 250 Ωcm and the 2 kΩcm diode will be discussed. Here it is essential that the boron concentration near to the highly doped p^+ Cz substrate increase to very large values. But this transition from the epitaxial bulk material to the p^+ substrate is smooth due to the out-diffusion of boron from the Cz substrate into the epitaxial layer during the high temperature steps in the fabrication process. This leads to a small increase of the depletion depth for bias voltages larger than the voltage for full depletion as extracted from C-V measurements together with an increase of the substitutional boron concentration $[B_s]$. Assuming now a similar creation rate of the B_iO_i defect as described in section D which depends on the local Boron concentration $[B_s]$ the increase of the B_iO_i concentration above full depletion can be qualitatively explained.

Considering a one-dimensional model for a diode, the B_iO_i

concentration can be described by:

$$[B_iO_i](w(V)) = \frac{\int_0^{w(V)} [B_iO_i](x)dx}{w(V)} \quad (16)$$

where $w(V)$ is the voltage dependent depletion depth. Assuming that the B_iO_i defect is homogeneously distributed in the bulk of diode, the evaluated concentration of the corresponding TSC peak $[B_iO_i]_{TSC}$ can be separated into two terms, the concentration of the bulk ($[B_iO_i]_{bulk}$) and an additional component ($[B_iO_i]_{add}$) from the region above full depletion (the value extracted from C-V measurement), i.e. $(w(V > V_{fd}) > d)$:

$$[B_iO_i]_{TSC}(w(V)) = [B_iO_i]_{bulk} + [B_iO_i]_{add}(w(V)) \quad (17)$$

with

$$[B_iO_i]_{add}(w(V)) = \frac{\int_d^{w(V)} ([B_iO_i]'(x) - [B_iO_i]_{bulk})dx}{w(V)} \quad (18)$$

where $[B_iO_i]'$ is the concentration in the region above fully depletion. Here the effective doping concentration N_{eff} is strongly increasing with bias (see Fig. 2b). Assuming that in this region N_{eff} is given by the local boron concentration $[B_s]$, the introduction of B_iO_i can be described by eq.(23) and eq.(24) presented in section D.

Taking both equations into account the increase of $[B_iO_i]_{add}$ can be estimated by:

$$\frac{\sum_{V_0=20V}^{V_{max}} ([\Phi_{eq} \cdot g_{B_iO_i}(N_{eff}(V)) - [B_iO_i]_{bulk}] \cdot \Delta w(V))}{w(V)} \quad (19)$$

where the $N_{eff}(V)$ are given by eq.(4) and $w(V)$ by eq.(5) the sums runs from V_0 = 20 V (near to full depletion voltage V_{fd}) up to V_{max} = 100 V in steps of 5 V.

In Fig. 7 the B_iO_i as function of bias voltage V near to and above full depletion is plotted for the 250 Ωcm and 2 kΩcm diode (09-73, 12-74) including the different annealing steps. The presented curves are the result of fits of eq.(19) to the measured data taken at the annealing step of 16 min at 80 ^{o}C.

The generation rate of interstitial silicon g_I, the substitutional carbon concentration $[C_s]$ and $[B_iO_i]_{bulk}$ are considered as free parameters in the fit of eq.(19) to the data of both sensors (250 Ωcm and 2 kΩcm). The resulting parameters of the fits are: $g_I = 6.28 \pm 0.5$ cm^{-1}, $[C_s] = (7.20 \pm 1) \times 10^{15}$ cm^{-3}, $[B_iO_i]_{bulk} = (2.91 \pm 0.1) \times 10^{13}$ cm^{-3} for 2 kΩcm. And $g_I = 6.00 \pm 0.5$ cm^{-1}, $[C_s] = (1.21 \pm 0.1) \times 10^{16}$ cm^{-3}, $[B_iO_i]_{bulk} = (9.64 \pm 0.1) \times 10^{13}$ cm^{-3} for 250 Ωcm. These values are different compared to those presented in section D. A possible reason might be that the studied transition region between the EPI and the highly doped Cz-material with the position dependent boron concentration $[B_s]$ behaves quite different compared to the EPI bulk material.

The $[BiOi]_{bulk}$ values extracted from TSC measurements at V = 20 V are included in TABLE III for both sensors.

C. Isochronal annealing behavior of B_iO_i

After the isothermal annealing at 80 °C for 180 min of the 50 Ωcm diode 06-71 an isochronal annealing study was performed. The procedure started at 100 °C with an annealing time of 15 min continued in 10 °C steps up to 190 °C. I-V and C-V measurements were recorded before the TSC measurements. While from the C-V characteristics the effective doping concentration N_{eff} was determined, the B_iO_i concentrations were evaluated from the TSC spectra for each annealing step. The resulting values are plotted in Fig. 8 versus the annealing temperature. The concentration of the B_iO_i is nearly constant with a value of about 3.3×10^{13} cm^{-3} up to 150 °C and start to anneal out at 160 °C decreasing to a value of 1.5×10^{12} cm^{-3} at 190 °C. On the other hand the effective space charge density N_{eff} stays nearly constant between 100 °C and 150 °C (1.01×10^{14} cm^{-3} to 1.1×10^{14} cm^{-3})

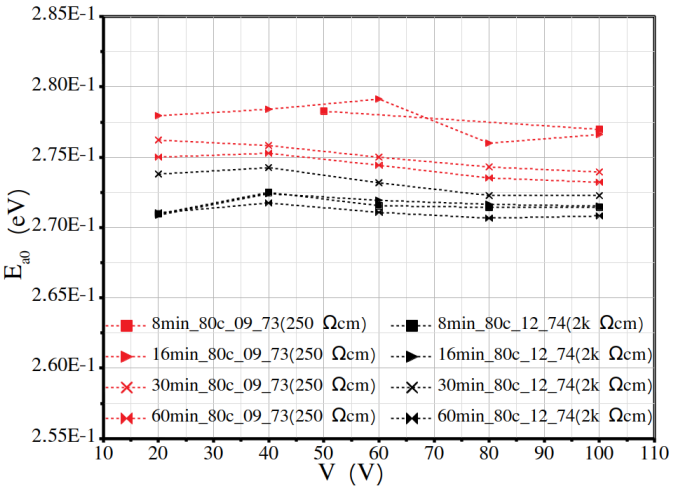

Figure 6: Zero field activation energy E_{a0} versus bias voltage of B_iO_i defect extracted from TSC spectra of the 250 Ωcm diodes (09-73) and 2 kΩcm diodes (12-74) and all annealing steps at 80 ^oC.

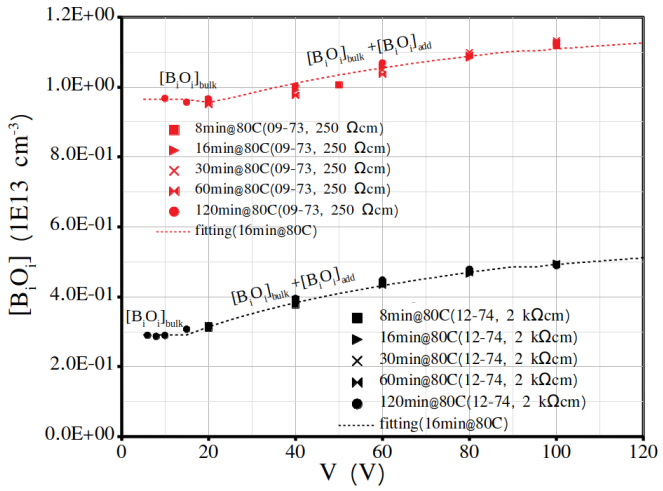

Figure 7: B_iO_i concentration as function of bias voltage (V) for the 250 Ωcm diode (09-73) and 2 kΩcm diode (12-74) extracted from TSC spectra measured after annealing steps between 8 min and 120 min at 80 ^{o}C. The curves are the result of fits of eq.(19) to the data. The parameters are presented in the text.

TABLE III

Properties of B_iO_i defect for isothermal annealing steps. (E_{a0} [eV], ΔE_a [eV], N_t [10^{13} cm^{-3}])
$E_{a0} \pm 1\% E_{a0}$ [eV], $N_t \pm 1\% N_t$ [10^{13} cm^{-3}]

Label	Diode 06-71			Diode 09-73			Diode 12-74		
Nominal resistivity	50 Ωcm			250 Ωcm			2 kΩcm		
	E_{a0}	ΔE_a	N_t	E_{a0}	ΔE_a	N_t	E_{a0}	ΔE_a	N_t
8min@80°C	0.288	≤ 0.005	3.2	0.278	≈ 0	0.95	0.272	≈ 0	0.31
16min@80°C	0.289	≤ 0.005	3.2	0.278	≈ 0	0.96	0.272	≈ 0	0.31
30min@80°C	0.283	≤ 0.005	3.3	0.275	≈ 0	0.95	0.273	≈ 0	0.32
60min@80°C	0.282	≤ 0.005	3.3	0.274	≈ 0	0.95	0.271	≈ 0	0.32

and increases for higher temperatures. Comparing the increase of N_{eff} with the decrease of the B_iO_i concentration ($[B_iO_i]$) one finds that a change of N_{eff} (ΔN_{eff}) is about two times the change of $[B_iO_i]$. This result is expected because the creation of B_iO_i changes the space charge by a factor 2, i.e. the negatively charged boron dopant (B_s) is transformed into the positively charged defect B_iO_i. More information can be gained from the isochronal annealing behavior of defects. If a first order process is assumed for the annealing-out of a defect it can be described by:

$$N_{t,i} = N_{t,i-1}(T_{ann,i-1}) \times \exp\left(-k_i \Delta t\right) \quad (20)$$

where $N_{t,i}$ is the concentration of B_iO_i for the annealing step i, $N_{t,i-1}(T_{ann,i-1})$ the concentration at step i-1 for the annealing temperature at this step and Δt the constant annealing time of 15 min. The frequency factors k_i are given by the Arrhenius relation:

$$k_i = k_0 \exp\left(\frac{-E_A}{k_B T_{ann,i-1}}\right) \quad (21)$$

E_A is the activation energy for the annealing-out of B_iO_i and k_B the Boltzmann constant. Taking the B_iO_i concentrations for the different annealing temperatures larger than 150 °C, which are plotted in Fig. 8, the frequency factors k_i were evaluated according to eq.(20). The Arrehnius plot k_i versus $1/(k_B T_{ann,i-1})$ is shown in Fig. 9. From a linear fit to the data the activation energy E_A [eV] and the frequency factor k_0 [s^{-1}] were extracted resulting in:

$$E_A = 1.35 \pm 0.01 \text{ [eV]}$$
$$k_0 = (2.58 \pm 0.5) \times 10^{11} \text{ [s}^{-1}\text{]}$$

Our result for the activation energy is close to values from 1.35 eV to 1.40 eV presented in [22], [33] – [35]. The error of E_a and k_0 are the results of the estimated error of the k_i values ($\pm 1\% \cdot k_i$) in eq.(21). The frequency factor k_0 depends on the content of boron, carbon and oxygen in the material. When the carbon concentration is relatively small then according to [33] the value of k_0 is determined by the ratio of the oxygen concentration to that one of boron ($[O]/[B]$). The larger this ratio is the less is the B_iO_i annealing rate due to re-trapping of interstitial boron by oxygen. As seen from Fig. 9 this ratio is in the 50 Ωcm epitaxial material smaller compared to $[O]/[B] \approx 200$ observed in the material used by Makarenko [33] or Feklisova [35].

D. Introduction rate of B_iO_i

In Ref. [9] the acceptor removal effect in LGAD and HV-CMOS sensors as well as p-type diodes is parameterized

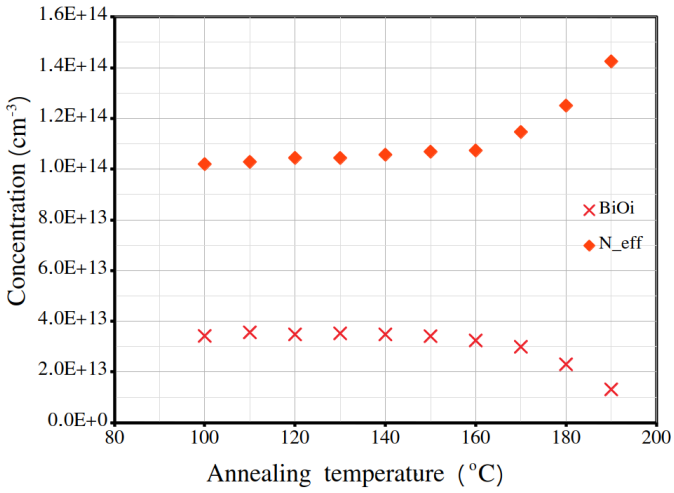

Figure 8: Dependence of the effective doping density N_{eff} and the B_iO_i defect concentration on the isochronal annealing temperature for the 50 Ωcm diode (06-71) after exposure to 4.3×10^{13} cm^{-2} 23 GeV protons

with an exponential function including an acceptor removal coefficient c_A. For small fluence values the acceptor removal component can be approximated by:

$$N_{eff}(\Phi_{eq}) = N_{eff,0} \exp\left(-c_A \Phi_{eq}\right) \approx N_{eff,0} - g_B \Phi_{eq} \quad (22)$$

where $N_{eff,0}$ is the initial doping concentration and $g_B = c_A \times N_{eff,0}$ the initial acceptor removal rate. In our case the acceptor removal rate has to be identified with the removal rate of electrically active boron and should be strongly correlated with the introduction rate of boron related defects, which can be extracted from TSC measurement by:

$$g(B_iO_i) = \frac{[B_iO_i]}{\Phi_{eq}} \quad (23)$$

Where $[B_iO_i]$ is B_iO_i concentration after irradiation to Φ_{eq}. The most likely created defect is the B_iO_i defect complex [9], [24] taking into account that in our silicon material the oxygen concentration is much larger compared to the carbon and boron content ($[O_i] \gg [C_s]$, $[B_s]$). The introduction rate of the B_iO_i defect is plotted in Fig. 10 as function of the initial doping concentration $N_{A,0}$. Included in the figure are data obtained from TSC measurements presented by A. Himmerlich et al. [36] and DLTS spectra measured by I. Pintilie et al. [37]. All TSC data are in very good agreement. The observed increase with $N_{eff,0}$ is expected according to the initial acceptor removal rate g_B (see above) but at higher

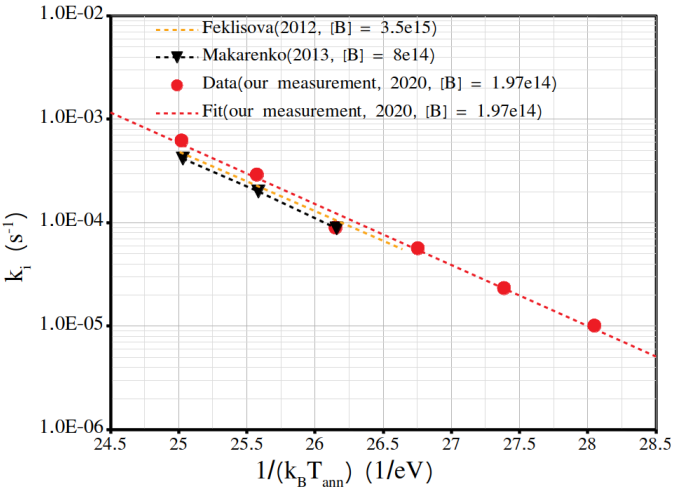

Figure 9: Arrehnius plot k_i versus $1/(k_BT)$. The k_i values were evaluated according to eq.(20) for the temperature interval from 130^{o}C to 190^{o}C. For comparison the data of L. F. Makarenko et al. [33] derived from diodes with an initial doping of $[B] \approx 8 \times 10^{14}$ cm^{-3} and O. V. Feklisova et al. [35] evaluated from diodes with a doping of $[B] \approx 3.5 \times 10^{15}$ cm^{-3} are also presented in the figure

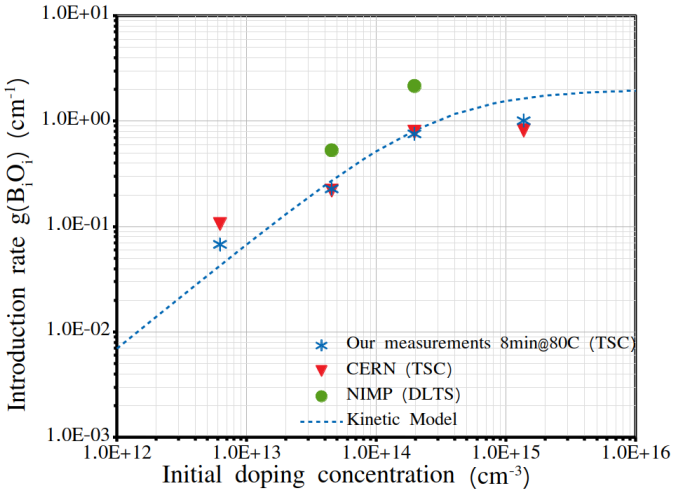

Figure 10: Development of the B_iO_i introduction rate $g_{B_iO_i}$ as function of the initial doping density $N_{eff,0}$. Our introduction rates in the plot are mean values taken from all isothermal annealing steps and the fluence value of 4.3×10^{13} cm^{-2} 23 GeV protons. Included are data of the other team members (see text).The dashed line represents the defect kinetic model calculation according to eq.(24) with parameters given in the text

$N_{eff,0}$ a saturation occurs. Such a behavior can be explained with the help of a simplified defect kinetics model [9], [38] where the assumption is made that the silicon interstitials (I) which escape from the primary displacement damage can react with substitutional boron (B_s) or carbon (C_s). In a so-called Watkins replacement mechanism both atoms become themselves interstitials ($I + B_s \xrightarrow{k_{IB}} B_i$, $I + C_s \xrightarrow{k_{IC}} C_i$), migrate through the lattice and can further react with other impurities like oxygen O_i creating thus e.g. B_iO_i or C_iO_i. If all silicon interstitials (I) end up only in these two defects their concentration ratio $[C_iO_i]/[B_iO_i]$ should reflect the ratio $(k_{IC}/k_{IB}) \times [C_s]/[B_s]$, where the ratio of the capture coefficient of carbon k_{IC} and boron k_{IB} has been evaluated to be $(k_{IC}/k_{IB}) \approx 1/7$ [38]. Finally the introduction rate of B_iO_i can be described by [9]:

$$g_{B_iO_i} \approx g_I \times \left(1 + \frac{k_{IC}[C_s]}{k_{IB}[B_s]}\right)^{-1} \quad (24)$$

The generation rate of interstitial related defects had been observed for high resistivity material to be about 1-3 cm^{-1} [39]. For our material we assume g_I = 2 cm^{-1} and $[C_s]$ = 2×10^{15} cm^{-3} [9], [38]. With these values eq.(24) results in the dashed line presented in Fig. 10. As can be seen from Fig. 10 the predicted introduction rate increases with the initial doping concentration nearly linear up to about 3×10^{14} cm^{-3} and tends to saturation above some 1×10^{16} cm^{-3}. Why the generation rate from DLTS are larger compared to results from TSC measurements is not clear and also results for LGAD sensors which are much larger than expected by this model cannot be explained so far [1], [2].

V. Conclusion

The boron-oxygen defect B_iO_i has been investigated in p-type epitaxial silicon diodes with different resistivities and exposed to 23 GeV protons. For all diodes isothermal annealing studies at 80 °C had been performed up to 120 min and for a 50 Ωcm diode an isochronal annealing followed in order to get information on the annealing-out of the B_iO_i. The macroscopic properties (current related damage parameter $\alpha(T_{ann}, t_{ann})$ and N_{eff}) were obtained from current-voltage (I-V) and capacitance-voltage (C-V) measurements. The α-values decrease with the annealing time as expected and the change of N_{eff} is quite small which correlates with the nearly constant concentration of the B_iO_i defect. The properties of the B_iO_i defect were studied by TSC measurements for different trap filling procedures (different T_0) and bias voltages during the heating up period. The observed temperature shift of the B_iO_i peak for different bias voltages is a clear indication for the so-called Poole-Frenkel effect. From a detailed analysis of the B_iO_i TSC signal the defect parameter for the zero field activation energy E_{a0}, the capture cross section σ_n, defect concentration N_t and energy shift ΔE_a due to clustering were extracted which are summarized in TABLE III. These results for the different isothermal annealing steps show that the activation energy slightly depends on the initial doping, the cross section is constant, ΔE_a is very small between 0-3 meV. But the concentration extracted from diodes irradiated to the same fluence depends strongly on the initial doping. Isochronal annealing studies were only performed for one 50 Ωcm diode irradiated to a fluence of $\Phi_{eq} = 4.3 \times 10^{13}$ cm^{-2}. The concentration of B_iO_i (N_t) versus annealing temperature from TSC was used to determine the activation energy for annealing-out

of the B_iO_i being E_A = 1.35 eV and a frequency factor of $k_0 = 2.58 \times 10^{11}$ s^{-1} was derived. On the other hand the increase of N_{eff} at temperatures above 150 °C correlates with the annealing-out of B_iO_i where the change of N_{eff} is about two times the change of B_iO_i reflecting the fact that for the creation of one positively charged B_iO_i one negatively charged substitutional boron atom B_s is removed. Finally, the generation rate of B_iO_i ($g_{B_iO_i}(N_{eff,0})$) is presented together with data of other groups and compared with a defect kinetics model [9], [38]. It is shown that $g_{B_iO_i}$ increases with the initial doping up to some 1×10^{14} cm^{-3} and tends to saturation for higher values.

It should be mentioned that the acceptor removal coefficient c_A (see eq.(22)) evaluated from our B_iO_i introduction rates are comparable with data derived from irradiated p-type sensors including HV-CMOS devices in a wide range of initial doping densities (see for example reference [9] and cited literature therein). But the scattering of the data is quite large despite the known difference between proton and neutron irradiated devices. On the other hand macroscopic and first microscopic studies on radiation damaged LGADs had resulted in much larger generation rates for boron related defects compared to our results obtained for epitaxial material [1], [2], [9]. This problem has to be investigated in further experiments.

ACKNOWLEDGMENT

This work has been carried out in the framework of the RD50 Collaboration. The project has received funding from the European Unions Horizon 2020 Research and Innovation program under Grant Agreement no. 654168. C. Liao would like to thank the Deutsche Forschungsgemeinschaft (DFG, German Research Foundation) under Germany's Excellence Strategy – EXC 2121 „Quantum Universe“ – 390833306 and Professor Z. Li for support his stay at the University of Hamburg. I. Pintilie acknowledge the funding received through IFA-CERN-RO 5/2019 project. Z. Li acknowledge the funding received through the Key Scientific and Technological Innovation Project of Shandong Province under Grant No. 2019 TSLH 0316, and the project of Yantai Insitute for the exchange of Driving Forces under Grants No. 2019XJDN002.

REFERENCES

[1] G. Kramberger, et al., “Radiation effects in Low Gain Avalanche Detectors after hadron irradiations,” *JINST*, vol. 10, no. 07, pp. P07006–P07006, Jul, 2015, DOI: 10.1088/1748-0221/10/07/p07006

[2] M. Ferrero, et al., “Radiation resistant LGAD design,” *Nucl. Instrum. Methods Phys. Res. A*, vol. 919, pp. 16–26, 2019, DOI: https://doi.org/10.1016/j.nima.2018.11.121

[3] A. Affolder, et al., “Charge collection studies in irradiated HV-CMOS particle detectors,” *JINST*, vol. 11, no. 04, pp. P04007–P04007, Apr, 2016, DOI: 10.1088/1748-0221/11/04/p04007

[4] E. Cavallaro, et al., “Studies of irradiated AMS H35 CMOS detectors for the ATLAS tracker upgrade,” *JINST*, vol. 12, no. 01, pp. C01074–C01074, Jan, 2017, DOI: 10.1088/1748-0221/12/01/c01074

[5] B. Hiti, et al., “Charge collection properties in an irradiated pixel sensor built in a thick-film HV-SOI process,” *JINST*, vol. 12, no. 10, pp. P10020–P10020, Oct, 2017, DOI: 10.1088/1748-0221/12/10/p10020

[6] I. Mandić, et al., “,Neutron irradiation test of depleted CMOS pixel detector prototype,” *JINST*, vol. 12, no. 02, pp. P02021–P02021, Feb, 2017, DOI: 10.1088/1748-0221/12/02/p02021

[7] B. Hiti, et al., “Charge collection in irradiated HV-CMOS detectors,” *Nucl. Instrum. Methods Phys. Res. A*, vol. 924, pp. 214–218, 2019, DOI: https://doi.org/10.1016/j.nima.2018.07.022

[8] I. Mandić, et al., “E-TCT measurements with passive CMOS pixel detectors on RD50-MPW1 chips from LFoundry,” RD50 Workshop, CERN, November 2018

[9] M. Moll, “Acceptor removal - Displacement damage effects involving the shallow acceptor doping of p-type silicon devices,” *PoS*, vol. Vertex2019, no. 027, pp. 1-12, Sep 2020, DOI: 10.22323/1.373.0027

[10] Institute of Electronic Materials Technology (ITME), Warsaw, Poland

[11] CiS Forschungsinstitut für Mikrosensork GmbH, Erfurt, Germany

[12] C. T. Sah, et al., “Thermal and optical emission and capture rates and cross sections of electrons and holes at imperfection centers in semiconductors from photo and dark junction current and capacitance experiments,” *SOLID STATE ELECTRON*, vol. 13, no. 6, pp. 759–788, Apr, 1970, DOI: https://doi.org/10.1016/0038-1101(70)90064-X

[13] I. Pintilie, et al., “Thermally stimulated current method applied on diodes with high concentration of deep trapping levels,” *APPL PHYS LETT*, vol. 78, no. 4, pp. 550-552, 2001, DOI: 10.1063/1.2832646

[14] M. G. Buehler, “Impurity centers in pn junctions determined from shifts in the thermally stimulated current and capacitance response with heating rate,” *SOLID STATE ELECTRON*, vol. 15, no. 1, pp. 69–79, 1972, DOI: https://doi.org/10.1016/0038-1101(72)90068-8

[15] M. Moll, “Radiation damage in silicon particle detectors: Microscopic defects and macroscopic properties,” PhD-Thesis, University of Hamburg, July 1999, DESY-THESIS-1999-040

[16] I. Pintilie, et al., “Stable radiation-induced donor generation and its influence on the radiation tolerance of silicon diodes,” *Nucl. Instrum. Methods Phys. Res. A*, vol. 556, pp. 197–208, 2006, DOI: https://doi.org/10.1016/j.nima.2005.10.013

[17] G. A. M. Hurkx, et al., “Intrinsic concentration, effective densities of states, and effective mass in silicon,” *IEEE Trans. Electron Devices*, vol. 39, no. 2, pp. 331-338, Feb. 1992, DOI: 10.1109/16.121690

[18] J. Zhang, “X-ray Radiation Damage Studies and Design of a Silicon Pixel Sensor for Science at the XFEL,” PhD-Thesis, University of Hamburg, June 2013, DESY-THESIS-2013-18

[19] A. Junkes, “Influence of radiation induced defect clusters on silicon particle detectors,” PhD-Thesis, University of Hamburg, July 2011, DESY-THESIS-2011-031

[20] E. Fretwurst, et al., “Determination of the p-spray profile for n+p silicon sensors using a MOSFET,” *Nucl. Instrum. Methods Phys. Res. A*, vol. 866, pp. 140-149, 2017, DOI: doi.org/10.1016/j.nima.2017.05.046

[21] J. Schwandt, et al., “Silicon detectors, Radiation damage, Time-dependent weighting field,” *Nucl. Instrum. Methods Phys. Res. A*, vol. 9942, pp. 162418, 2019, DOI: https://doi.org/10.1016/j.nima.2019.162418

[22] P. M. Mooney, et al., “Defect energy levels in boron-doped silicon irradiated with 1-MeV electrons,” *Phys. Rev. B*, vol. 15, no. 8, pp. 3836–3843, Apr, 1977, DOI: 10.1103/PhysRevB.15.3836

[23] J. Adey, et al., “Formation of BiOi, BiCs, and BiBsHi defects in e-irradiated or ion-implanted silicon containing boron,” *APPL PHYS LETT*, vol. 83, no. 4, pp. 665–667, June, 2003, DOI: https://doi.org/10.1063/1.1595728

[24] L. C. Kimerling, et al.,Interstitial defect reactions in silicon, Materials Science Forum Vols. 38-41(1989) pp 141-150. DOI: https://doi.org/10.4028/www.scientific.net/MSF.38-41.141

[25] J, Frenkel, “On pre-breakdown phenomena in insulators and electronic semi-conductors,” *Phys. Rev.*, vol. 54, no. 8, pp. 647–648, Oct, 1938, DOI: 10.1103/PhysRev.54.647

[26] J. L. Hartke, “The three-dimensional Poole-Frenkel effect,” *J APPL PHYS*, vol. 39, no. 10, pp. 4871–4873, 1968, DOI: 10.1063/1.1655871

[27] I. Pintilie, et al., “Cluster related hole traps with enhanced-field-emission—the source for long term annealing in hadron irradiated Si diodes,” *APPL PHYS LETT*, vol. 92, no. 2, pp. 024101, 2008, DOI: 10.1063/1.2832646

[28] M. A. Green, et al., “Stable radiation-induced donor generation and its influence on the radiation tolerance of silicon diodes,” *J APPL PHYS*, vol. 67, no. 6, pp. 2944–2954, 1990, DOI: 10.1063/1.345414

[29] C. Besleaga, et al., “Bistability of the BiOi complex and its implications on evaluating the acceptor removal,” *arXiv*, pre-print, 2021, DOI: https://arxiv.org/abs/2102.06537

[30] A. Scheinemann, et al., “TCAD-based DLTS simulation for analysis of extended defects,” Phys. Status Solidi A 211, No. 1, 136-142 (2014) / DOI 10.1002/pssa.201300233

[31] E. M. Donegani, et al., “Study of point-and cluster-defects in radiation-damaged silicon,” *Nucl. Instrum. Methods Phys. Res. A*, vol. 898, pp. 15–23, 2018, DOI: https://doi.org/10.1016/j.nima.2018.04.051

[32] C. Liao, et al., "The boron-oxygen (BiOi) defect complex induced by irradiation with 23 GeV protons in p-type epitaxial silicon diodes," 37th RD50 Workshop, Nov 2020, Zagreb
[33] L. F. Makarenko, "Formation and annealing of boron-oxygen defects in irradiated silicon and silicon-germanium n+–p structures," AIP Conference Proceedings. Vol. 1583. No. 1. American Institute of Physics, 2014. DOI: https://doi.org/10.1063/1.4865618
[34] K, Aurangzeb, et al., "Role of the impurities in production rates of radiation-induced defects in silicon materials and solar cells," *J APPL PHYS*, vol. 90, no. 3, pp. 1170–1178, 2001, DOI: 10.1063/1.1384855
[35] O. V. Feklisova, et al., "Annealing kinetics of boron-containing centers in electron-irradiated silicon," *Semiconductors*, vol. 47, no. 2, pp. 228–231, 2013. DOI: https://doi.org/10.1134/S1063782613020085
[36] A. Himmerlich, et al., "Defect investigations of electron irradiated p-type Si sensors," 37th RD50 Workshop, Nov 2020, Zagreb
[37] I. Pintilie, et al., "Structural, compositional and defect studies on hadron irradiated B-doped silicon diodes," 37nd RD50 Workshop, Nov 2020, Zagreb
[38] L. F. Makarenko, et al., "Formation of a Bistable Interstitial Complex in Irradiated p-Type Silicon," *PHYS STATUS SOLIDI A*, vol. 216, no. 17, pp. 1900354, 2019, DOI: https://doi.org/10.1002/pssa.201900354
[39] G. Davies, et al., "Radiation damage in silicon exposed to high-energy protons," *Phys. Rev. B*, vol. 73, no. 16, pp. 165202, Apr, 2006, DOI: 10.1103/PhysRevB.73.165202